



## Bithiazole inhibitors of PI4KB show broad-spectrum antiviral activity against different viral families

Maria Grazia Martina<sup>a</sup>, Vincent Carlen<sup>b</sup>, Sarah Van der Reysen<sup>a</sup>, Elena Bianchi<sup>c</sup>,  
Noemi Cabella<sup>c</sup>, Emmanuele Crespan<sup>c</sup>, Marco Radi<sup>a,\*\*</sup>, Valeria Cagno<sup>b,\*</sup>

<sup>a</sup> Dipartimento di Scienze Degli Alimenti e Del Farmaco (DipALIFAR), Università Degli Studi di Parma, Viale Delle Scienze, 27/A, 43124, Parma, Italy

<sup>b</sup> Institute of Microbiology, University Hospital of Lausanne, University of Lausanne, 1011, Lausanne, Switzerland

<sup>c</sup> Istituto di Genetica Molecolare, IGM-CNR "Luigi Luca Cavalli-Sforza", Via Abbiategrasso 207, 27100, Pavia, Italy

### A B S T R A C T

Broad-spectrum antivirals can be extremely important for pandemic preparedness. Targeting host factors dispensable for the host but indispensable for the virus can result in high barrier to resistance and a large range of viruses targeted. PI4KB is a lipid kinase involved in the replication of several RNA viruses, but common inhibitors of this target are mainly active against members of the *Picornaviridae* family. Herein we describe the optimization of bithiazole PI4KB inhibitors as broad-spectrum antivirals (BSAs) active against different members of the *Picornaviridae*, *Coronaviridae*, *Flaviviridae* and *Poxviridae* families. Since some of these viruses are transmitted via respiratory route, the efficacy of one of the most promising compounds was evaluated in an airway model. The molecule showed complete viral inhibition and absence of toxicity. These results pave the road for the development of new BSAs.

### 1. Introduction

The paucity of effective antiviral drugs with a broad-spectrum activity, combined with long development timelines, unsuited for rapid epidemic or pandemic scenarios, poses a significant challenge. Additionally, the emergence of viral resistance to existing antiviral therapies further boosts complexity. Respiratory viruses stand out as leading causes of global mortality ([Global Burden of Disease Study, 2015](#)), often coalescing to exacerbate illness severity. Rhinovirus, respiratory syncytial virus (RSV), influenza viruses, and coronaviruses, among others, frequently co-infect, intensifying the clinical burden and complicating treatment approaches ([Dallmeyer et al., 2024](#); [Goka et al., 2015](#); [Heimonen et al., 2024](#), [Martin et al., 2012](#)). Furthermore, despite traditionally causing mild respiratory or gastrointestinal infections, some members of the *Picornaviridae* can cause neurological complications ([Anastasina et al., 2017](#); [Syage et al., 2023](#); [Wu et al., 2023](#); [Poelaert et al., 2023](#)). For instance, Enterovirus (EV)-A71 has been associated with severe complications such as neurogenic pulmonary edema, acute flaccid paralysis, and brainstem encephalitis, sometimes resulting in death ([Chang et al., 1999](#); [Lum et al., 1998](#); [Ooi et al., 2010](#)). COVID-19 pandemic evidenced instead how a respiratory virus can cause multiple extra-pulmonary manifestations, leading for instance to cardiovascular alterations, dermatologic, and neurological symptoms. This scenario not

only challenges current treatment strategies but also emphasizes the need for innovative interventions and the importance of addressing the unique challenges of infections and co-infections in clinical practice and research efforts.

One potential strategy to circumvent the main limitations of common antiviral drugs targeting viral proteins involves targeting host factors, specifically proteins essential for viral replication but dispensable for host cell viability. Among these, phosphatidylinositol kinases (PIKs) emerge as pivotal players in the formation of replication organelles (ROs), critical for the replication of positive-strand RNA viruses (+RNA viruses). Notably, phosphatidylinositol 4-kinase type III $\beta$  (PI4KB), a host lipid kinase, stands out for its central role in RNA replication across viruses belonging to the family of *Picornaviridae*. During viral replication, the 3A structural protein indirectly recruits PI4KB to its replication organelles (RO) via its interaction with host factors that bind to PI4KB. Several studies have shown that PI4KB inhibitors exhibit strong antiviral effects on Picornaviruses ([Arita et al., 2015](#), [Cheong et al., 2023](#), [McPhail and Burke, 2023](#), [Mejdrová et al., 2015](#), [Mejdrová et al., 2017](#), [Spickler et al., 2013](#), [van Der Schaar et al., 2013](#)). A substantial endeavor has been directed in recent years toward discovering novel chemotypes for the inhibition of PI4KB, leading to the development of numerous small molecules with inhibitory activity mainly against viruses of the *Picornaviridae* family ([Fig. 1](#)). One of the first inhibitors, PIK-93, was

\* Corresponding author.

\*\* Corresponding author.

E-mail addresses: [marco.radi@unipr.it](mailto:marco.radi@unipr.it) (M. Radi), [valeria.cagno@chuv.ch](mailto:valeria.cagno@chuv.ch) (V. Cagno).

<https://doi.org/10.1016/j.antiviral.2024.106003>

Received 27 May 2024; Received in revised form 29 July 2024; Accepted 8 September 2024

Available online 10 September 2024

0166-3542/© 2024 The Authors. Published by Elsevier B.V. This is an open access article under the CC BY license (<http://creativecommons.org/licenses/by/4.0/>).

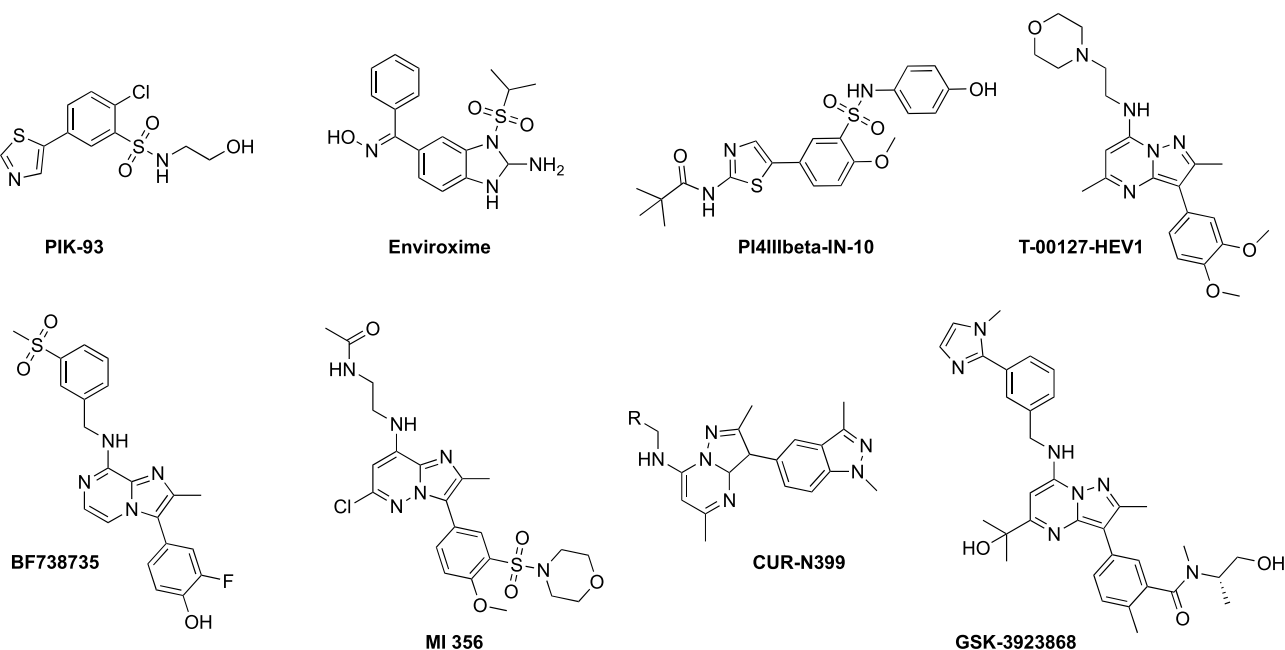


Fig. 1. Representative PI4KB inhibitors endowed with inhibitory activity against viruses of the Picornaviridae family.

initially thought to specifically target PI4KB but exhibited cross-reactivity with other enzymes. Despite early inhibitors initially lacking specificity, PIK-93 has undergone structural modifications resulting in improved versions with enhanced selectivity and lower toxicity, exemplified by compounds such as PI4KIIIbeta-IN-9 and PI4KIIIbeta-IN-10, which have shown to inhibit *in vitro* enterovirus replication. Enviroxime, another PI4KB inhibitor, has long been known as an inhibitor of the *in vitro* replication of rhinoviruses, enteroviruses and HCV. Similarly, inhibitors, like T-00127-HEV1 and BF738735, showed the ability to fight viruses like poliovirus and CVB3, along with anti-HCV activity. Additionally, the development of derivatives based on the imidazo [1,2-b]pyridazine scaffold, resulted in compounds like MI356. This compound emerges as the most potent and selective PI4KB inhibitor identified to date, with  $IC_{50} = 0.98$  nM and a significant inhibitory effect toward CVB3, HRV1, and HCV1b. Noteworthy, CUR-N399 exerts broad-spectrum antiviral activity *in vitro* against various viruses within the *Picornaviridae* family and promotes survival from a lethal infection with EV-A71 in mice. Its therapeutic efficacy is substantiated by the fact that it has entered phase I clinical trials to evaluate safety, tolerability, and pharmacokinetics profile in healthy adults ([ClinicalTrials.gov](https://clinicaltrials.gov), 2022). To date, the effectiveness of PI4KB inhibitors in combating Rhinovirus culminates with GSK-3923868, a potent, selective, PI4KB inhibitor, for which a phase II clinical trial for the treatment of viral Chronic Obstructive Pulmonary Disease (COPD) exacerbations, linked to Rhinovirus infection, is currently recruiting subjects ([ClinicalTrials.gov](https://clinicaltrials.gov), 2023). These findings highlight that the majority of known PI4KB inhibitors have shown antiviral activity specifically against human rhinoviruses and enteroviruses (Li et al., 2024).

In this regard, bithiazole inhibitors of the host kinase PI4KB have been previously identified as promising antiviral candidates. They inhibit the replication of a panel of enteroviruses (EVs) representative of all major species: EV group A (EV71), group B (coxsackievirus B3, CVB3, and echovirus 11, ECHO11), group C (poliovirus 1, PV1), group D (enterovirus 68, EV68), rhinovirus group A (RV02) and rhinovirus group B (RV14) (Tassini et al., 2017, 2019). Within this bithiazole family, a few derivatives with a double aliphatic and polar functionalization on the right part of the central scaffold, have shown an extended spectrum of antiviral activity. As we described in a recent communication (Martina et al., 2021), these new derivatives blocked the replication of human rhinoviruses (RV), Zika virus (ZIKV) and SARS-CoV-2 at low

micromolar and sub-micromolar concentrations in absence of toxicity, demonstrating the potential of PI4KB inhibitors as broad-spectrum antiviral agents against diverse viral pathogens.

Building upon these preliminary results and on limited literature data showing that PI4KB is also involved in the replication of Zika virus (Ci et al., 2021) and SARS-CoV (Yang et al., 2012), herein we have expanded the collection of bithiazole PI4KB inhibitors to consolidate the antiviral data and their broad-spectrum of activity. Results showed that, unlike conventional PI4KB inhibitors reported in Fig. 1, PI4KB inhibitors based on the bithiazole scaffold demonstrated unparalleled activity against a wide range of clinically significant viruses belonging not only to the *Picornaviridae* family but also to the *Flaviviridae*, *Coronaviridae* and *Poxviridae* families. We further investigated the mechanism of action. Bithiazole derivatives act on SARS-CoV-2, Zika virus and RVA16 by inhibiting viral replication, and for RVA16 we proved the PI4KB-dependent inhibitory activity. Furthermore, we demonstrated that the efficacy of the bithiazole compounds can be further improved through combination with antivirals directly targeting the viruses and that their activity is retained in human-derived tissue models.

## 2. Materials and methods

### 2.1. Chemistry

All commercially available chemicals were purchased from Fisher Scientifics or Fluorochem and, unless otherwise noted, used without any previous purification. Solvents used for work-up and purification procedures were of technical grade. When required, the reactions were conducted under a nitrogen atmosphere using appropriate lines, techniques that require the use of syringes and septa, in well washed and dried flasks. The used anhydrous reaction solvents, dichloromethane, methanol, THF and acetonitrile, were distilled just before use. TLC was carried out using Merck TLC plates (silica gel on Al foils, SUPELCO Analytical). Where indicated, products were purified by silica gel flash chromatography on columns packed with Merck Geduran Si 60 (40–63  $\mu$ m).  $^1\text{H}$  and  $^{13}\text{C}$  NMR spectra were recorded on BRUKER AVANCE 400 MHz spectrometers. Chemical shifts ( $\delta$  scale) are reported in parts per million relative to TMS; coupling constants  $J$  are reported in hertz (Hz).  $^1\text{H}$ -NMR spectra are reported in this order: multiplicity and number of protons; signals were characterized as: s (singlet), d (doublet), dd

(doublet of doublets), ddd (doublet of doublet of doublets), t (triplet), m (multiplet), bs (broad signal). Elemental analyses were performed on a by using a FlashSmart CHNS analyzer (Thermo Fisher) with gas-chromatographic separation. All final compounds were >95% pure as determined by elemental analysis (within 0.4% of the theoretical values). Low resolution mass spectrometry measurements were performed on an Agilent 6100 Series InfinityLab LC/MSD iQ, Single Quadrupole analyzer and are reported in the form of (m/z).

## 2.2. In vitro kinase inhibition assays

Recombinant full length, HIS6-tagged PI4KIII $\beta$  and recombinant full length, N-terminal FLAG-tagged full-length human PI3KR1 (p110 $\alpha$  - GenBank® Accession Number U79143 - and human p85 $\alpha$  - no tag; GenBank® Accession Number XM\_043865) were purchased from Pro-Qinase (Germany).

### 2.2.1. Assay conditions

PI4KB and PI3KR1 reactions were performed in 10  $\mu$ L using 20 mM Tris-HCl pH 7.5, 0.125 mM EGTA, 2 mM DTT, 0.04% Triton, 3 mM MgCl<sub>2</sub>, 3 mM MnCl<sub>2</sub>, 20  $\mu$ M ATP, 0.01  $\mu$ Ci  $\gamma$ -P33 ATP, 200  $\mu$ M Pi:3 PS, 10% DMSO, 0.4 ng/ $\mu$ L of PI4KIII $\beta$  and 7.6 ng/ $\mu$ L of PI3KR1. All reactions were performed at 30 °C for 10 min.

Reactions were stopped depleting the remaining ATP by adding 12.5  $\mu$ L of ADP-Glo Reagent (Promega, USA) with 10 mM MgCl<sub>2</sub> for 40 min at room temperature shaking the tubes. 25  $\mu$ L of Kinase Detection Reagent (Promega, USA) were added and incubated for 30 min at room temperature. Luminescent signal was detected on a GloMax plate reader (Promega, USA). IC<sub>50</sub> values were obtained according to Equation (1), where  $v$  is the measured reaction velocity,  $V$  is the apparent maximal velocity in the absence of inhibitor,  $I$  is the inhibitor concentration, and IC<sub>50</sub> is the 50% inhibitory concentration.

$$v = V / \{1 + (I / IC_{50})\} \quad (1)$$

### 2.2.2. Lipidic substrate preparation

PI: phosphatidylinositol (Sigma); PS: 2-Oleoyl-1-palmitoyl-sn-glycero-3-phospho-L-serine (Sigma). PI and PS were dissolved in chloroform/methanol 9:1 and mixed at a 1:3 ratio. After chloroform/methanol evaporation, water was added to 1:62.5 w/v and the mixture sonicated to clarity.

## 2.3. Cells and viruses

Hela, VeroE6, Huh7 were grown in DMEM with 4.5 g/l D-Glucose, while Calu3 were grown in EMEM 1X both supplemented with 110 mg/L Sodium Pyruvate (Gibco, ThermoFisher Scientific) and 10% of fetal bovine serum (FBS) and penicillin/streptomycin (pen/strep) 100 UI/ml (P/S) at 37 °C in an incubator with 5% CO<sub>2</sub>.

Rhinovirus (RV) 16 and 54, Enterovirus (EV) D68 (Fermon strain), EVA71 (BrCr strain) were a kind gift from the laboratory of Prof Taparel of the University of Geneva. Zika virus (ZIKV), Yellow Fever Virus (YFV), West Nile Virus (WNV) were obtained from Labor Spiez. Monkeypox virus (MPXV) was isolated from a clinical specimen of the University Hospital of Lausanne. SARS-CoV-2 was obtained by isolation of a clinical strain (Omicron BA.1) from the University Hospital of Lausanne as previously described (Mathez and Cagno, 2021). Human coronavirus 229e (HCoV-229e) was obtained from ATCC (VR-740). Stocks were obtained by collecting supernatant of infected cells when cells displayed extensive cytopathic effect, clarified at stored at -80 °C.

## 2.4. Cell toxicity assay

Cell viability was measured by 3-(4,5-dimethylthiazol-2-yl)-2,5-diphenyl tetrazolium bromide (MTT). Confluent cell seeded in 96-well plates were incubated with different concentrations of compounds in

duplicate under the same experimental conditions described for the antiviral assays. Absorbance was measured using a Microplate Reader at 570 nm. The effect on cell viability at different concentrations of the compounds was expressed as a percentage, by comparing the absorbance of treated cells with the one of cells incubated with equal concentrations of solvent in medium. The 50% cytotoxic concentration (CC<sub>50</sub>) and 95% confidence intervals (CIs) were determined using Prism software (Graph-Pad Software, San Diego, CA).

## 2.5. Antiviral assay with rhinovirus and enterovirus

Hela cells (1.6  $\times$  10<sup>4</sup> cells per well) were seeded in 96 well plate. The following day the cells were infected with RV (16 and 54) or EV68 at MOI 0.01 for 1h at 33 °C, the inoculum was removed and serial dilutions of the compounds in medium were added on cells. 48hpi cells were fixed with methanol and stained with RV VP3 monoclonal antibody (G47A, ThermoFisher) or Enterovirus pan-monoclonal antibody (L66J, ThermoFisher) and IgG anti-mouse conjugated with horseradish peroxidase. Subsequently tetramethylbenzidine (TMB) was added on the cells and blocked with 1N Hydrochloric Acid. The absorbance was read at 450 nm. The percentage of infection was calculated by subtracting the value of cells not infected and then dividing the absorbance in the infected and treated well to the mean of the absorbance in infected wells. Experiments with EVA71 were done as previously described for EVD68 but on VeroE6 and at 37 °C.

## 2.6. Antiviral assay with SARS-CoV-2

Vero-E6 cells (1  $\times$  10<sup>5</sup> cells per well) were seeded in 24-well plate. Cells were infected with SARS-CoV-2 (MOI, 0.001 PFU/cell) for 1 h at 37 °C. The monolayers were then washed and overlaid with 0.4% avicel gp3515 in medium containing 2.5% FBS and serial dilutions of the compounds. Three days after infection, cells were fixed with 4% formaldehyde and stained with crystal violet solution containing ethanol. Plaques were counted, and the percent inhibition of virus infectivity was determined by comparing the number of plaques in treated wells with the number in untreated control wells. 50% effective concentration (EC<sub>50</sub>) was calculated with Prism 9.1 (GraphPad).

Calu-3 cells (4  $\times$  10<sup>4</sup> cells per well) were seeded in 96-well plate. Cells were infected with SARS-CoV-2 (MOI 0.1 PFU/cell) for 1 h at 37 °C. The monolayers were then washed and overlaid with medium containing serial dilutions of compounds. At 48 hpi, cells and supernatant were lysed, and viral RNA was extracted with EZNA total RNA kit (Omega Bio-tek). SARS-CoV-2 RNA was quantified by RT-qPCR with the QuantiTect Kit (Qiagen, 204443) with Sarbeco E gene primers and probe in a QuantStudio 3 thermocycler (Applied Biosystems). Percent inhibition of virus infectivity was determined by comparing viral load in treated wells with the viral load in untreated control wells. EC<sub>50</sub> was calculated with Prism 9.1 (GraphPad).

## 2.7. Antiviral assay with flaviviruses

Vero-E6 cells or Huh7 (1  $\times$  10<sup>5</sup> cells per well) were seeded in 24-well plate. Vero-E6 were infected with ZIKV or WNV while Huh7 were infected with YFV (MOI 0.001 PFU/cell) for 1 h at 37 °C. The monolayers were then washed and overlaid with medium containing methylcellulose and serial dilutions of the compounds. Three days after infection, cells were fixed and stained with a crystal violet solution containing ethanol. Plaques were counted, and the percent inhibition of virus infectivity was determined by comparing the number of plaques in treated wells with the number in untreated control wells. 50% effective concentration (EC<sub>50</sub>) was calculated with Prism 9.1 (GraphPad).

Alternatively, Vero-E6 and Huh7 cells (1  $\times$  10<sup>4</sup> cells per well) were seeded in 96 well plates and infected with Zika virus respectively MOI 0.01 and MOI 0.1 after 1h the inoculum was removed and serial dilutions of the compounds in medium were added on cells. 72 hpi cells

were fixed with methanol and stained with primary antibody mouse anti-flavivirus envelope protein antibody (4G2, Abcam) and IgG anti-mouse conjugated with horseradish peroxidase. Subsequently tetramethylbenzidine (TMB, Sigma) was added on the cells and blocked with 1N Hydrochloric Acid. The absorbance was read at 450 nm. The percentage of infection was calculated by subtracting the value of cells not infected and then dividing the absorbance in the infected and treated well to the mean of the absorbance in infected wells.

## 2.8. Antiviral assay with 229e virus

Huh7 cells (105 cells per well) were seeded in 24-well plate. Cells were infected with HCoV-229e (MOI, 0.002 PFU/cell) for 1 h at 37 °C. The monolayers were then washed and overlaid with medium containing 0.4% avicel gp3515 and serial dilutions of the compounds. Three days after infection, cells were fixed and stained with a crystal violet solution containing ethanol. Plaques were counted, and the percent inhibition of virus infectivity was determined by comparing the number of plaques in treated wells with the number in untreated control wells. 50% effective concentration (EC<sub>50</sub>) was calculated with Prism 9.1 (GraphPad).

## 2.9. Antiviral assays with monkeypox virus

Vero-E6 (1 × 10<sup>5</sup> cells per well) were seeded in 24-well plate. Cells were infected with MPXV (MOI 0.002 PFU/cell) for 1h at 37 °C. The monolayers were then washed and overlaid with medium containing 0.5% methylcellulose and serial dilutions of the compounds. Two days after infection, cells were fixed and stained with a crystal violet solution containing ethanol. Plaques were counted, and the percent inhibition was determined by comparing the number of plaques in treated wells with the number in untreated control wells. 50% effective concentration (EC<sub>50</sub>) was calculated with Prism 9.1 (GraphPad).

## 2.10. Viral RNA quantification

Cells (105 cells per well) were seeded in 24wp. The following day the cells were infected with RV16 MOI 0.1 1hpi the inoculum was removed, and compounds (5 μM) were immediately added on cells, or added 2, 4, 6 hpi. Alternatively, cells were treated 1h before infection, or only during the hour of infection and subsequently the compounds were washed out. Similar procedures were followed for SARS-CoV-2 and Zika virus. 24hpi the supernatant was harvested, and cells were lysed. RNA was extracted and viral RNA amplified with RT-qPCR. For RV were used: primer forward 5'-AGCCTGCGTGGCKGCC-3' et 5'-CYN-AGCCNTGCGTGG-3', primer reverse 5'-GAA ACA CGG ACA CCC AAA GTA GT-3', probe 5'-CTC CGG CCC CTG AAT GYG GCT AA-3'; for SARS-CoV-2 primer forward. For ZIKV were used: primer forward 5'-CTTGAGTGCTTGTGATT-3', primer reverse 5'-CTCCTCCAGTGTT-CATTT-3', probe 5'-AGAAGAGAATGACCACAAAGATCA-3'. For SARS-CoV-2 E-sarbeco primers and probe were used.

## 2.11. EV71 replicon

The plasmid pSVA-EV71-N772-NL encoding a replicon of EV71 expressing nanoluciferase instead of the P1 region was obtained by Koike lab (Tokyo Metropolitan Institute of Medical Science). The plasmid was linearized with Sall (New England Biolabs) and vitro transcribed with RiboMax kit (Promega) and the RNA was purified (E.Z. N.A. Total RNA extraction kit, Omega Biotech). Vero cells were plated in 96 well plate at a density of 8 × 10<sup>3</sup> cells/well, the following day the cells were treated with the compounds at 5 or 1 μM. 18 h post transfection the RNA of the EV71 replicon was transfected with Lipofetamine RNAiMax (Thermo Fisher scientific). The luminescence was read 24 h post transfection with NanoGlo luciferase assay system (Promega).

## 2.12. Resistance selection

Hela cells (3 × 10<sup>5</sup> cells per well) were seeded in 6-well plate. At the first passage, cells were infected with RV16 (MOI 0.01) for 1 h at 37 °C. The inoculum was removed and compounds or rupintrivir at the respective EC<sub>50</sub> were added on the wells, one well was left untreated. Supernatants were collected when the cells displayed extensive cytopathic effect (3–6 dpi) and clarified at 2 × 10<sup>3</sup> rpm for 5 min. Each sample was quantified by TCID method on Hela cells. For the following passages, cells were infected with the previous corresponding passage (MOI 0.01) and the concentrations of compounds were doubled when possible.

## 2.13. Sequencing

RNA was extracted from isolated viral stocks with E.Z.N.A total RNA (Omega Bio-Tek). Maxima H Minus cDNA Synthesis (Thermofisher) and Platinum II Taq (Thermofisher) were used as RT-PCR kits. The 3C amplification was performed with designed primers (Fwd 5'-AGT GAC ATT CAA GGA CCG CA-3', Rev 5'-CCA AAG CTT CCA AGC CAT CC-3'). PCR products were Sanger sequenced by Microsynth.

## 2.14. I92T experiments

Plasmids containing the RV16 WT (pR16.11) or with I92T mutation (pR16 I92T) previously described (Roulin et al., 2018) were obtained by the Greber laboratory (University of Zurich). The plasmids were linearized with SacI (New England Biolabs) and vitro transcribed with RiboMax kit (Promega), the RNA was purified (Total RNA extraction kit, Omega Biotech) and it was transfected in HeLa cells with Lipofetamine RNAiMax (Thermo Fisher Scientific). When the cells displayed extensive cytopathic effect supernatants were collected and purified. After titration, the compounds were tested as described in the antiviral assay section.

## 2.15. Mucilair experiments

Tissues were obtained from Epithelix (Geneva, Switzerland). For all experiments, epithelia were prepared by pool of donors. Before inoculation with the viruses, MucilAir tissues were incubated in 250 μL of PBS Ca<sup>2+</sup>Mg<sup>2+</sup> (PBS<sup>++</sup>) for 20 min at 37 °C. Infection was done with 10<sup>6</sup> RNA copies/tissue with RVA16. At 3 h after incubation at 33 °C, tissues were rinsed three times with MucilAir medium to remove non-adsorbed virus and the compound 2a was added at a final concentration of 10 μM. Every 24 h, 200 μL of MucilAir medium was applied to the apical face of the tissue for 20 min at 33 °C for sample collection, followed by apical treatment with 2a. Viral load was determined by qPCR as described previously or by titration of the tissue supernatant. In parallel experiments were done in absence of infection and the apical daily wash was analyzed for LDH release.

## 2.16. Statistics and data analysis

Experiments were performed in duplicate and from two to four independent experiments as stated in the figure legends. Results are shown as mean and SEM. The EC<sub>50</sub> and CC<sub>50</sub> values for inhibition curves were calculated by regression analysis using the program GraphPad Prism version 9.1 to fit a variable slope sigmoidal dose-response curve. The synergism data were generated with Synergy Finder and evaluated through the Zero interaction potency (ZIP) model which is based on the change in the potency of the dose-response curves between individual drugs and their combinations. ZIP synergy score above 10 is considered as synergism, between -10 and 10 as additive, lower than 10 as antagonistic.

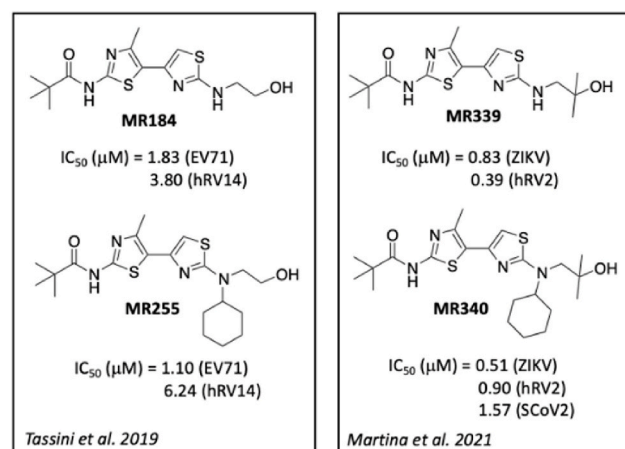
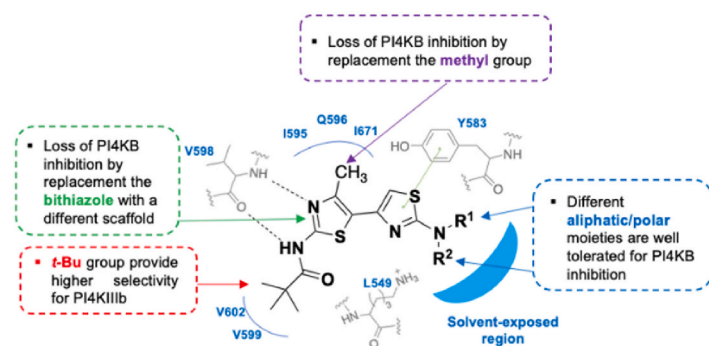
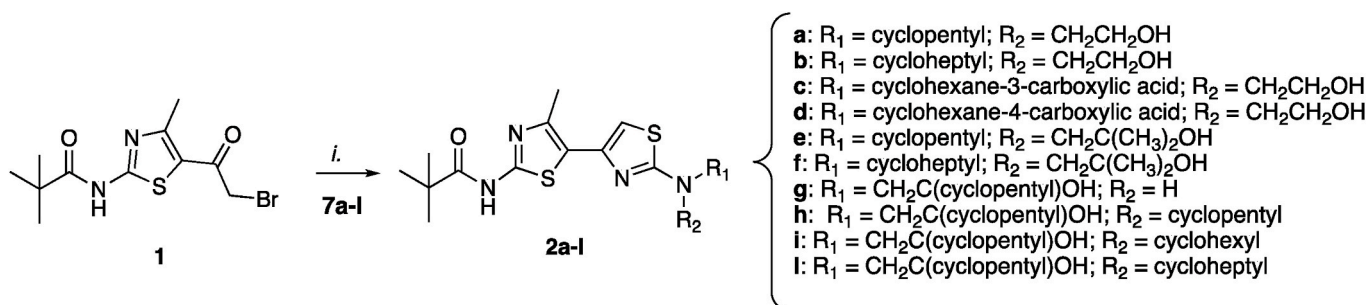


Fig. 2. Structure-activity relationships (SAR) of PI4KB-targeting bithiazoles and antiviral activities of recently published double aliphatic/polar functionalized derivatives.



Scheme 1. Reagents and conditions: i. EtOH, reflux, 3–8h.

### 3. RESULTS and DISCUSSION

#### 3.1. Synthesis

A thorough exploration of the structure-activity relationships for bithiazole antivirals targeting PI4KB has been conducted in the last few years, allowing to identify the key pharmacophoric moieties required for the potent and selective inhibition of this specific lipid kinase (Fig. 2). Notably, these studies have revealed critical SARs insights: replacing the bithiazole scaffold with different scaffolds or changing the methyl group in C4 position resulted in a loss of PI4KB inhibition. However, variations in different aliphatic/polar moieties at the R<sup>1</sup> and R<sup>2</sup> positions were well tolerated and the introduction of a t-butyl group on the left side of the scaffold remarkably enhanced the selectivity for PI4KB inhibition.

As reported in a recent communication, the bithiazole derivatives bearing aliphatic and/or polar functional groups on the right part of the bithiazole scaffold (e.g. MR339 and MR340) were able to inhibit the replication viruses belonging to different families, such as RV 2 (*Picornaviridae* family), ZIKV (*Flaviviridae* family) and SARS-CoV2 (*Coronaviridae* family). Similar compounds (MR184 and MR255) were also previously investigated for their antiviral activity against the *Picornaviridae* family only. These insights from previous SAR studies guided us in synthesizing a series of new aliphatic/polar functionalized bithiazole derivatives, by exploiting previously reported synthetic procedures (Martina et al., 2021, 2022), to better understand the peculiar broad antiviral activity of this class of PI4KB inhibitors.

Target compounds **2a-h** were simply prepared by reacting functionalized thioureas (**7a-l**) with a common intermediate (**1**) under reflux conditions in ethanol (Scheme 1). The key intermediate **1** already possesses essential structural features, crucial for the high selectivity and activity toward PI4KB, namely the tert-butyl group on the left part of the

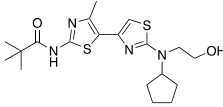
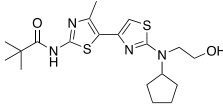
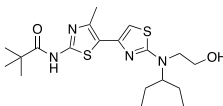
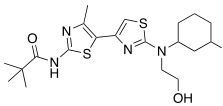
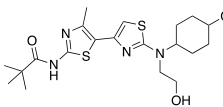
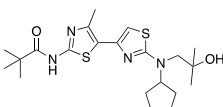
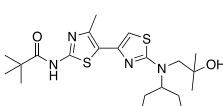
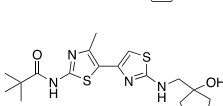
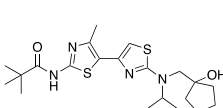
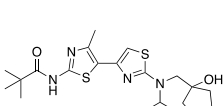
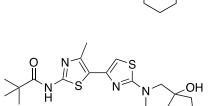
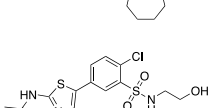
molecule, the C4-methyl group and the central bithiazole core (Fig. 2). A total of 10 new molecules were thus prepared and characterized. The detailed procedures for the synthesis of non-commercial thioureas, target compounds and characterization data are reported in Supporting Information file and in Supplementary Fig. 1.

#### 3.2. Kinase inhibition

The newly synthesized compounds were tested for PI4KB inhibition to evaluate if the modifications resulted in altered kinase inhibition. Selectivity towards PI4KB was assessed evaluating compounds activity against PI3KR1 (Table 1). All compounds inhibited PI4KB in the low-to sub-micromolar range, with **2g** being the most active one. From this and previous studies, it is clear that the bithiazole core is crucial for the inhibition of PI4KB and that the tButyl group on the left part of the molecule confers selectivity for PI4KB over other lipid kinases (e.g. PI3KR1). The methyl group in C4 of the thiazole is also needed for the inhibition of PI4KB, since its replacement with a trifluoromethyl group has previously shown to generate molecules with no activity against PI4KB (Barbieri et al., 2024). The right part of the molecules (R<sub>1</sub> and R<sub>2</sub> in Fig. 2) allows instead the introduction of different substituents without losing the inhibitory activity against PI4KB. In particular, we have shown here that increasing the steric bulk of aliphatic substituents on the right side of the bithiazole scaffold or including polar moieties (OH, CO<sub>2</sub>H) in different positions, is well tolerated and always leads to PI4KB inhibitors with low micromolar activity.

Conversely, none of the compounds displayed a significant activity against PI3KR1 when tested at 100 μM: only compound **2c** showed a 39% residual activity against PI3KR1, which is however higher than the PI4KB residual activity (8%) (Table 1). Despite some variation in residual activity, the synthesized compounds generally showed a stronger

**Table 1**  
Inhibitory effect of target compounds **2a-1** against PI4KB and PI3KR1.

ID		residual activity	IC <sub>50</sub>	residual activity
		(100 μM)	(μM) ± SD	(100 μM)
		PI4KB		PI3KR1
<b>2a</b>		4%	1.5 ± 0.12	100%
<b>2b</b>		3.20%	1.18 ± 0.15	54%
<b>2c</b>		8%	3.56 ± 0.26	39%
<b>2d</b>		3.40%	0.4 ± 0.08	97%
<b>2e</b>		10%	0.55 ± 0.05	57%
<b>2f</b>		16.8%	1.69 ± 0.71	51%
<b>2g</b>		9%	0.27 ± 0.04	66%
<b>2h</b>		5%	0.311 ± 0.079	53%
<b>2i</b>		10%	0.30 ± 0.04	59%
<b>2l</b>		7%	0.297 ± 0.051	54%
<b>PIK-93</b>		2%	0.052 ± 0.006	

inhibition of PI4KB over PI3KR1, supporting their selectivity for PI4KB as discussed in our previous publications.

### 3.3. Antiviral activity of bithiazole derivatives

The compounds were then tested for their antiviral activity by

adding them 1 hour after infection with RVA16 and EVD68 on HeLa cells; Zika virus on VeroE6 and confirmed on Huh7 cells; SARS-CoV-2 on VeroE6 and confirmed on Calu-3 cells. Enviroxime, a known PI4KB inhibitor, was included as a control compound. It efficiently inhibited RVA16, EVD68 and SARS-CoV-2 but did not inhibit ZIKV at the tested doses (Table 2). All compounds, except, **2c** showed inhibitory activity against RVA16 and EVD68, which is in line with the well known correlation between PI4KB and viral replication of the *Picornaviridae* family. The lack of activity of **2c** against RVA16 and EVD68 might be due to its lower potency against PI4KB and a possible intramolecular interaction between the CO<sub>2</sub>H and OH groups inside the cell, which may mask these pharmacophoric moieties or generate an inactive derivative. As discussed in a previous publication (Martina et al., 2021), the presence of derivatives with potent PI4KB inhibitory activity and no inhibition of SCoV2 (e.g. **2h,i** or **MR340**) is a clear indication of a multi-target antiviral mechanism for this class of compounds. Despite the additional targets involved in the antiviral activity of these molecules are still unknown, it is noteworthy that five derivatives (**2a,b,d,f,g**) retained activity against ZIKV and seven derivatives (**2a,b,d,e,f,g,l**) against SARS-CoV-2 at the tested doses, proving that bithiazole PI4KB inhibitors act indeed as BSAs. A clear rationalization of their structure-activity-relationships for the different viruses will require further studies on the target identification that is out of the scope of the present manuscript.

After careful consideration, we selected **2a** and **2g** for further analysis, since they retained activity against all the tested viruses. While compounds such as **2l** demonstrated specific antiviral profiles, we prioritized compounds with the potential to inhibit multiple viruses, in line with the focus of the present work.

### 3.4. Spectrum of activity of selected compounds

To evaluate the spectrum of the antiviral activity of two selected compounds, additional viruses belonging to the same viral families tested in the initial screening were tested: namely EVA71 and RVA54 for the *Picornaviridae*; HCoV-229e for the *Coronaviridae*; WNV and YFV for the *Flaviviridae*. Additionally, MPXV, belonging to the *Poxviridae*, was tested since members of the *Poxviridae* were previously reported to require PI4P for replication (Kolli et al., 2015). The compounds retain activity against all viruses tested except for WNV for which no inhibition was present at any tested dose (Table 3), in line with previous reports in which the virus was shown to be independent from PI4KB (Martin-Acebes et al., 2011). However, enviroxime shows activity against all viruses tested except WNV and YFV (Table 3). This suggests that targeting PI4KB is not sufficient to mediate inhibition of *Flaviviridae* members, as ZIKV was also not affected (Table 2).

### 3.5. Evaluation of the mechanism of action

Next, we evaluated if the compound **2a**, which showed inhibition of all viruses, was active against RVA16, ZIKV and SARS-CoV-2 when added before, during or after infection. In the first two conditions, the compound was washed out after 1h incubation. This evaluation was conducted after a single cycle of replication of the viruses as an indication of its mechanism of action. For the three viruses, the best inhibitory activity was achieved when **2a** was added post infection (Fig. 3A–C), consistently with a role in viral replication. For SARS-CoV-2 the inhibition was significant also when the compound was added before or during infection (Fig. 3B) possibly suggesting multiple modes of action against the virus, for instance the involvement of PI4KB in viral entry (Yang et al., 2012).

### 3.6. Evaluation of RVA16 activity and PI4KB dependency

PI4KB is best known for its role in the formation of the replication organelles in the *Picornaviridae* family. Furthermore, EVD68 and RVA16

**Table 2**  
Antiviral activity of bithiazole derivatives.

	Hela			VeroE6			Huh7		VeroE6		Calu3	
	EC <sub>50</sub> RVA16	EC <sub>50</sub> EVD68	CC <sub>50</sub>	EC <sub>50</sub> ZIKV	CC <sub>50</sub>	EC <sub>50</sub> ZIKV	CC <sub>50</sub>	EC <sub>50</sub> SCoV2	CC <sub>50</sub>	EC <sub>50</sub> SCoV2	CC <sub>50</sub>	
<b>2a</b>	0.36	0.899	8.28	1.88	>50	4.06	11.1	3.92	>50	2.71	5.3	
<b>2b</b>	1.6	2.14	30.6	2.13	61.19	6.21	26	7.8	>50	3.99	5.21	
<b>2c</b>	n.a.	n.a.	36.9	n.a.				n.a.				
<b>2d</b>	1.55	3.22	>50	2.63	>50	6.51	7.13	5.67	>50	5.02	46.15	
<b>2e</b>	0.245	0.541	>50	n.a.	>50			9.67	>50	n.a.	>50	
<b>2f</b>	1.06	2.54	29.3	4.59	>50	5.58	19.3	1.4	>50	4.95	8.61	
<b>2g</b>	0.145	0.411	>50	2.02	25.7	1.64	15.9	4.43	25.7	11.2	>50	
<b>2h</b>	0.215	0.518	>50	n.a.	>50			n.a.	>50			
<b>2i</b>	0.393	0.841	49.8	n.a.	>50			n.a.	>50			
<b>2l</b>	0.346	0.884	45.5	n.a.	>50			9.66	>50	10.3	>50	
<b>Env</b>	0.042	0.154	44.3	n.a.	>50			0.57	>50			

EC<sub>50</sub> 50% effective concentration, CC<sub>50</sub> 50% cytotoxic concentration, EC<sub>50</sub> and CC<sub>50</sub> are expressed in  $\mu$ M. RVA16 Rhinovirus A16, EVD68 Enterovirus D68, ZIKV Zika Virus, SCoV2, SARS-CoV-2. n.a. not assessable (no inhibition was observed at the tested doses).

**Table 3**  
Spectrum of activity.

	Picornaviridae		Coronaviridae	Flaviviridae		Poxviridae
	EC <sub>50</sub> EVA71	EC <sub>50</sub> RVA54	EC <sub>50</sub> HCoV-229e	EC <sub>50</sub> WNV	EC <sub>50</sub> YFV	EC <sub>50</sub> MPOXV
<b>2g</b>	0.0511	0.149	0.941	n.a.	1.52	11.0
<b>2a</b>	0.318	0.200	0.550	n.a.	1.05	3.32
<b>Env</b>	0.0303	0.120	4.75	n.a.	n.a.	4.75

EC<sub>50</sub> 50% effective concentration, EC<sub>50</sub> is expressed in  $\mu$ M. EVA71, enterovirus A71; RVA54, Rhinovirus A54; HCoV-229e, Human coronavirus 229e; WNV, West Nile Virus; YFV, Yellow Fever Virus; MPOXV Monkeypox virus. n.a. not assessable (no inhibition was observed at the tested doses).

are the two viruses for which we observed the activity of most derivatives. Therefore, we performed additional experiments to verify that the mechanism of action of the compounds on this virus is compatible with what was previously reported. The compounds were added from 2 to 6 hours post-infection. Compounds **2a** and **2g** showed activity when added post-infection, and the inhibition was retained up to 6 hpi, confirming inhibition of replication, since both the RNA intracellular levels (Fig. 4A) and the release of infectious viruses are affected (Fig. 4B). Furthermore, the inhibition of the replication was verified in a system independent from cell entry or egress, with a EVA71 replicon in which the structural proteins are absent and replaced by nano luciferase in parallel with enviroxime (Fig. 4C).

To further verify the mechanism of action, RVA16 was grown in presence of increasing concentrations of selected compounds or rupintrivir, a 3C protease inhibitor which was tested up to phase II clinical trials (Nainwal, 2022) as control. After 7 passages it was possible to select for resistance against rupintrivir, verified both with a shift in the EC<sub>50</sub> (Table 4) and through sequencing of the 3C protease which evidenced the presence of 2 previously reported mutations: T130A and I160M. However, in presence of the compounds **2a** and **2g** the growth of the virus was hampered, and it was not possible to increase the selective pressure and consequently select for resistance (Supplementary Fig. 2). Therefore, we took advantage of a previously reported mutation (I92T) (Roulin et al., 2018) which was conferring resistance to PI4KB inhibitors to evaluate if we could observe a decrease of antiviral activity. Both **2a**, **2g** and enviroxime showed a decreased activity in presence of the mutation, further confirming the target (Fig. 4D). However, it is important to notice that the compounds retain activity in the submicromolar range also in presence of the mutation, in line with what previously reported (Roulin et al., 2018). Differently than the mutations in 3A protein, which are conferring resistance to PI4KB inhibitors by affecting the polyprotein processing (Arita, 2016; Melia et al., 2017), I92B mutation was associated to increased viral replication in presence of low levels of PI4KB. Subsequently we verified if the compounds were effective on the rupintrivir-resistant virus, the results are shown in Table 4 and show the lack of appearance of cross-resistance confirming different targets of the antiviral molecules.

Additionally, we tested for synergistic activity **2g** and rupintrivir

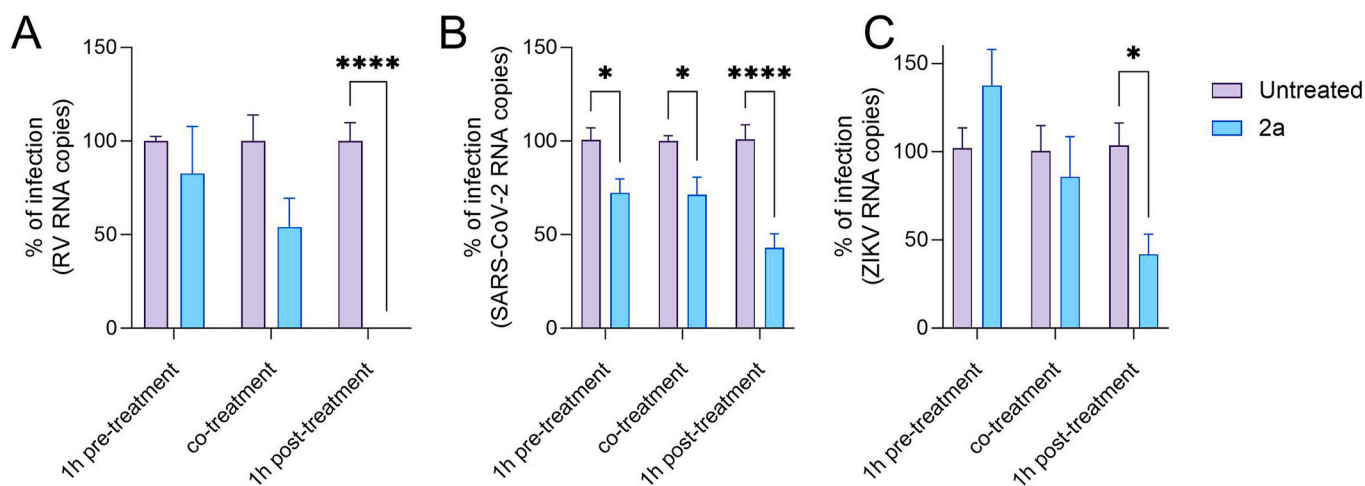


**Fig. 3.** Time of addition of **2a**. The compound (5  $\mu$ M for RVA16 and 10  $\mu$ M for SARS-CoV-2 and ZIKV) was added to cells either 1h before infection, or during infection and then washed out, or post-infection. The viral RNA amount was evaluated through qPCR in the cell lysates. The results are mean and SEM of three independent experiments. \* $p < 0.05$  \*\* $p < 0.01$ , \*\*\*\* $p < 0.001$ .

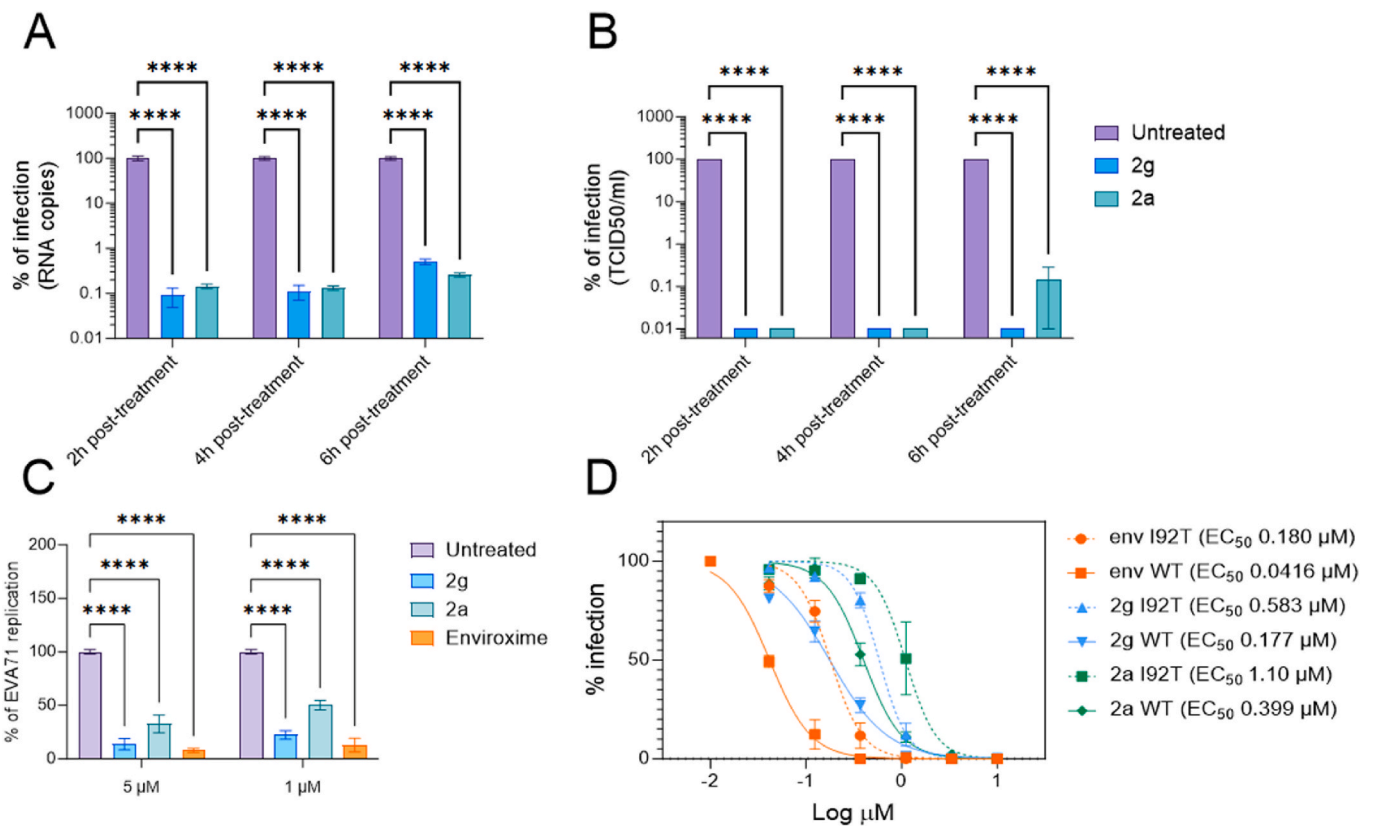


**Fig. 4.** Time of addition on RVA16. The selected compounds (5 μM) were added on cells at different time post-infection. The infectivity was evaluated through (A) titration of virus in the supernatant collected at 24hpi, or (B) by cell lysis and quantification of intracellular viral RNA. C) Vero cells were treated with 5 or 1 μM of **2a** or **2g** or enviroxime as positive control, 18h post treatment the RNA of EVA71 replicon was transfected and the luminescence was measured 24 later. The results are mean and SEM of three independent experiments. D) Antiviral activity on RVA16 and RVA16 with the point mutation I92T. Hela cells were infected with either RVA16 wild-type or with RVA16 with the mutation I92T. The infected cells were treated with serial dilution of enviroxime, **2g** and **2a**. The infection was evaluated 48hpi. Percentages of infection were calculated by comparing treated and untreated wells. The results are mean and SEM of three independent experiments. ENV: enviroxime \*\*p < 0.01, \*\*\*p < 0.005, \*\*\*\*p < 0.001.

**Table 4**  
Antiviral activity against rupintrivir-resistant virus.

	EC <sub>50</sub> vs RVA16 p7	EC <sub>50</sub> vs RUP p7
<b>2g</b>	0.098	0.099
<b>2a</b>	0.52	0.49
<b>rupintrivir</b>	0.00204	0.0144

The data are expressed in μM. RUP p7: RVA16 grown 7 times in presence of increasing concentrations of rupintrivir.

(Fig. 5) and we observed generally an additive effect, with some areas of synergistic effect (in red), proving the advantage of administering combinations of drugs with different targets. Further work could elucidate if the combination with other targets (i.e. targeting the capsid with pleconaril), could result in a better synergism.

Finally, we evaluated if the activity of **2g** was maintained in a human-derived respiratory tissue model. We infected the tissues with RVA16, and we treated them at 3hpi. The viral growth was evaluated by analysis of the apical daily washes of the tissues. The compound proved to be effective in reducing the viral replication quantified by RT-qPCR (Fig. 6A) and by viral titrations (Fig. 6B), completely abolishing viral growth. Importantly, the compound **2g** did not show cytotoxicity (Fig. 6C).

**4. Conclusion**

While conventional PI4KB inhibitors typically exhibit activity

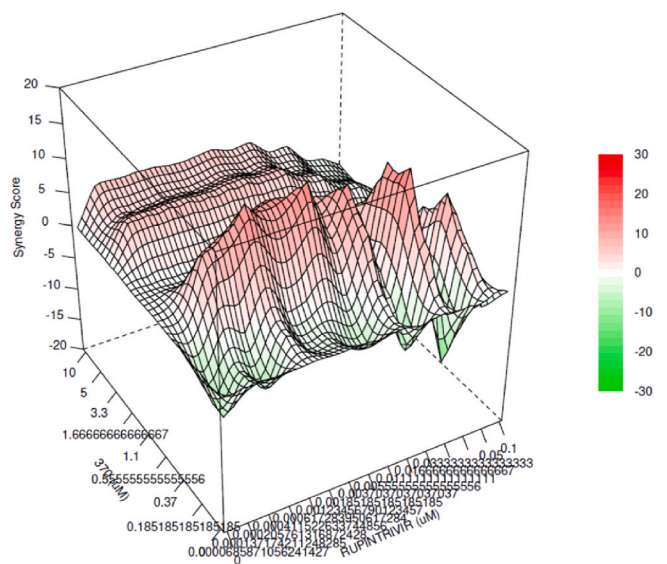


**Fig. 5.** Synergistic effect. Hela cells were infected with RVA16 and 1hpi treated with **2g** and rupintrivir with a matrix of concentrations (starting from 10 μM for **2g** and 0.1 μM for rupintrivir). The infectivity was evaluated 48hpi. The synergism was calculated with SynergyFinderPlus. Results are from 3 independent experiments.



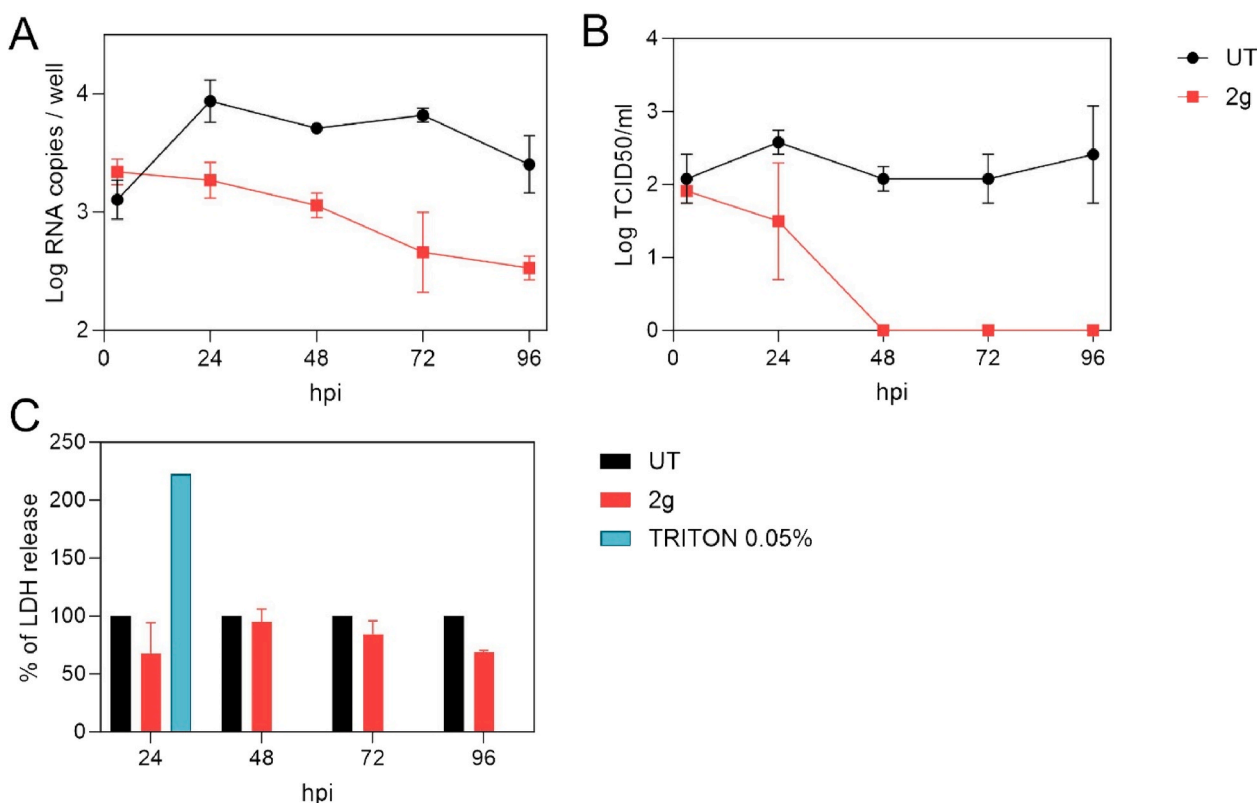


**Fig. 6.** Antiviral activity of compound **2g** in a human-derived tissue model. A-B) Mucilair tissues were infected with RVA16  $10^6$  rna copies. 3hpi the tissues were treated with  $10 \mu\text{M}$  of compounds **2g**. Every 24 h an apical wash was performed and collected after 20 min at  $37^\circ\text{C}$ . The supernatant was then used for viral RNA quantification (A) or for plaque assay (B). C) Mucilair tissues were treated with  $10 \mu\text{M}$  of compound **2g** or with 0.05% Triton. Every 24 h an apical wash was performed and collected after 20 min at  $37^\circ\text{C}$ . The supernatants were then evaluated for LDH release. The results are the mean and SEM of two independent experiments performed in duplicate. hpi: hours post-infection.

limited to the *Picornaviridae* family, our study showcases the feasibility of developing broad-spectrum antiviral compounds by targeting this crucial host target. By tweaking the solvent-exposed region of the bithiazole chemotype, we have developed ten compounds with potent antiviral activity against a wide range of clinically relevant viruses, belonging not only to the *Picornaviridae* family but also to the *Flaviviridae*, *Coronaviridae* and *Poxviridae* families. Although PI4KB is likely the primary target for these compounds, their effects can be complex due to the involvement of additional targets. Opportune modification of this chemical scaffold have previously proved to generate molecules acting at the same time on PI4KB and CFTR-F508del (Tassini et al., 2017, 2019) or PI4KB and Topoisomerase IV (Martina et al., 2022). The broad antiviral effect herein highlighted for some derivatives (e.g. **2a,b,d,f,g**) might thus be due to the inhibition of PI4KB plus an additional but still unknown target. Furthermore, variations in PI4KB expression levels across different cell lines may contribute to differences in the antiviral potency.

Our mechanistic studies, conducted on selected compounds **2a** and **2g**, both effective against all tested viruses, revealed intriguing insights into their mechanism of action. Time of addition of compound **2g** showed the best inhibitory activity against RVA16, ZIKV and SARS-CoV-2 when added post-infection. Surprisingly, significant inhibition of SARS-CoV-2 was also observed even when the compound was added before infection, suggesting potential multiple modes of action, involving PI4KB in viral entry. Evaluation of PI4KB dependency of these compounds was evaluated by employing the I92T mutation in 2B protein of RVA16, known to confer resistance to PI4KB inhibitors, like enviroxime. The reduction of activity of compounds **2a** and **2g** confirmed PI4KB involvement, although these compounds retained activity in the submicromolar range also in presence of the mutation.

Furthermore, **2a** and **2g** exhibited effectiveness against rupintrivir-resistant virus, suggesting a distinct mechanism compared to common 3C protease inhibitors. The additive and synergistic effects of **2g** in combination with rupintrivir highlight the potential benefits of targeting different viral components simultaneously. With respiratory transmission being a common route for many pathogens, **2g** demonstrated efficacy and safety in a respiratory human-derived tissue model, advocating for their topical administration to minimize systemic side effects and maximize localized concentration at the site of action.

Overall, the results reported in the present paper hold promise for the further development of bithiazole PI4KB inhibitors as broad-spectrum antivirals, allowing also improved *in vivo* safety through combination therapies or topical administration.

#### CRediT authorship contribution statement

**Maria Grazia Martina:** Writing – review & editing, Writing – original draft, Investigation. **Vincent Carlen:** Investigation. **Sarah Van der Reysen:** Investigation. **Elena Bianchi:** Investigation. **Noemi Cabella:** Investigation. **Emmanuele Crespan:** Supervision. **Marco Radi:** Writing – review & editing, Writing – original draft, Supervision, Project administration, Methodology, Funding acquisition, Data curation, Conceptualization. **Valeria Cagno:** Writing – review & editing, Writing – original draft, Supervision, Project administration, Methodology, Investigation, Funding acquisition, Data curation, Conceptualization.

#### Declaration of competing interest

The authors declare that they have no known competing financial interests or personal relationships that could have appeared to influence

the work reported in this paper.

## Data availability

Data will be made available on request.

## Acknowledgments

This work has been supported by the Novartis Foundation for Biomedical Research (grant n. 22A074, to V.C.) and by the Swiss National Science Foundation (grant n PZ00P3\_193,289 for the salary of V. C.). Financial support has been also provided by the Italian MUR, Ministero dell'Università e Ricerca to M.R. (PRIN 2022 project, cod. 2022TLZRXT; Funded by the European Union – Next Generation EU). This work was also partially supported by EU funding within the NextGenerationEU-MUR PNRR Extended Partnership initiative on Emerging Infectious Diseases (Project no. PE00000007, INF-ACT) to M. R. (INF-ACT Cascade Open Call 2023; COC-I- 2023-CNR). M.R. also thanks Andrea Cornacchione for partial technical assistance. E.C. and E. B. were supported by AIRC IG grant (Id: 24448).

## Appendix A. Supplementary data

Supplementary data to this article can be found online at <https://doi.org/10.1016/j.antiviral.2024.106003>.

## References

- Anastasina, M., Domanska, A., Palm, K., Butcher, S., 2017. Human picornaviruses associated with neurological diseases and their neutralization by antibodies. *J. Gen. Virol.* 98, 1145–1158. <https://doi.org/10.1099/jgv.0.000780>.
- Arita, M., 2016. Mechanism of poliovirus resistance to host phosphatidylinositol-4 kinase III beta inhibitor. *ACS Infect. Dis.* 2, 140–148. <https://doi.org/10.1021/acsinfecdis.5b00122>.
- Arita, M., Philipov, S., Galabov, A.S., 2015. Phosphatidylinositol 4-kinase III beta is the target of oxoglaucine and pachypodol (Ro 09-0179) for their anti-poliovirus activities, and is located at upstream of the target step of brefeldin A. *Microbiol. Immunol.* 59, 338–347. <https://doi.org/10.1111/1348-0421.12261>.
- Barbieri, F., Carlen, V., Martina, M.G., Sannio, F., Cancade, S., Perini, C., Restori, M., Crespan, E., Maga, G., Docquier, J.D., Cagno, V., Radi, M., 2024. 4-Trifluoromethyl bithiazoles as broad-spectrum antimicrobial agents for virus-related bacterial infections or co-infections. *RSC Med. Chem.* 15, 1589–1600. <https://doi.org/10.1039/d3md00686g>.
- Chang, L.Y., et al., 1999. Clinical features and risk factors of pulmonary oedema after enterovirus-71-related hand, foot, and mouth disease. *Lancet* 354 (9191), 1682–1686.
- Cheong, D.H.J., Yogarajah, T., Wong, Y.H., Arbrandt, G., Westman, J., Chu, J.J.H., 2023. CUR-N399, an inhibitor PI4KB, per il trattamento dell'infezione da Enterovirus A71. *Ricerca antivirale* 218, 105713. <https://doi.org/10.1016/j.antiviral.2023.105713>.
- Ci, Y., Yang, Y., Xu, C., Qin, C.F., Shi, L., 2021. Electrostatic interaction between NS1 and negatively charged lipids contributes to flavivirus replication organelles formation. *Front. Microbiol.* 12, 641059. <https://doi.org/10.3389/fmicb.2021.641059>.
- ClinicalTrials.gov, 2022. First-in-human clinical trial evaluating CUR-N399 in healthy volunteers. <https://clinicaltrials.gov/study/NCT05016687>.
- ClinicalTrials.gov, 2023. Efficacy and safety of GSK3923868 inhalation powder, during experimental human rhinovirus infection in participants with mild asthma. <https://clinicaltrials.gov/study/NCT05398198?intr=GSK-3923868&rank=1>.
- Dallmeyer, L.K., Schütz, M.L., Fragkou, P.C., Omony, J., Krumbain, H., Dimopoulou, D., Dimopoulou, K., Skevaki, C., 2024. Epidemiology of respiratory viruses among children during the SARS-CoV-2 pandemic: a systematic review and meta-analysis. *Int. J. Infect. Dis.* 138, 10–18. <https://doi.org/10.1016/j.ijid.2023.10.023>.
- Global Burden of Disease Study, C., 2015. Global, regional, and national incidence, prevalence, and years lived with disability for 301 acute and chronic diseases and injuries in 188 countries, 1990–2013: a systematic analysis for the Global Burden of Disease Study 2013. *Lancet* 386, 743–800. [https://doi.org/10.1016/S0140-6736\(15\)60692-4](https://doi.org/10.1016/S0140-6736(15)60692-4).
- Goka, E.A., Vallely, P.J., Mutton, K.J., Klapper, P.E., 2015. Single, dual and multiple respiratory virus infections and risk of hospitalization and mortality. *Epidemiol. Infect.* 143, 37–47. <https://doi.org/10.1017/S0950268814000302>.
- Heimonen, J., Chow, E.J., Wang, Y., Hughes, J.P., Rogers, J., Emanuels, A., O'Hanlon, J., Han, P.D., Wolf, C.R., Logue, J.K., Ogokeh, C.E., Rolles, M.A., Uyeke, T.M., Starita, L., Englund, J.A., Chu, H.Y., 2024. Risk of subsequent respiratory virus detection after primary virus detection in a community household study—king county, Washington, 2019–2021. *J. Infect. Dis.* 229, 422–431. <https://doi.org/10.1093/infdis/jiad305>.
- Kolli, S., Meng, X., Wu, X., Shengjuler, D., Cameron, C.E., Xiang, Y., Deng, J., 2015. Structure-function analysis of vaccinia virus H7 protein reveals a novel phosphoinositide binding fold essential for poxvirus replication. *J. Virol.* 89, 2209–2219. <https://doi.org/10.1128/JVI.03073-14>.
- Li, G., Wu, Y., Zhang, Y., Wang, H., Li, M., He, D., Guan, W., Yao, H., 2024. Research progress on phosphatidylinositol 4-kinase inhibitors. *Biochem. Pharmacol.* 220, 115993. <https://doi.org/10.1016/j.bcp.2023.115993>.
- Martin-Acebes, M.A., Blazquez, A.B., Jimenez de Oya, N., Escibano-Romero, E., Saiz, J. C., 2011. West Nile virus replication requires fatty acid synthesis but is independent on phosphatidylinositol-4-phosphate lipids. *PLoS One* 6, e24970. <https://doi.org/10.1371/journal.pone.0024970>.
- Lum, L.C., et al., 1998. Fatal enterovirus 71 encephalomyelitis. *J. Pediatr.* 133 (6), 795–798.
- Martin, E.T., Kuypers, J., Wald, A., Englund, J.A., 2012. Multiple versus single virus respiratory infections: viral load and clinical disease severity in hospitalized children. *Influenza Resp Viruses* 6, 71–77. <https://doi.org/10.1111/j.1750-2659.2011.00265>.
- Martina, M.G., Vicenti, I., Bauer, L., Crespan, E., Rango, E., Boccuto, A., Olivieri, N., Incerti, M., Zwaagstra, M., Allodi, M., Bertoni, S., Dreassi, E., Zazzi, M., Van Kuppeveld, F.J.M., Maga, G., Radi, M., 2021. Bithiazole inhibitors of phosphatidylinositol 4-kinase (PI4KIIIβ) as broad-spectrum antivirals blocking the replication of SARS-CoV-2, Zika virus, and human rhinoviruses. *ChemMedChem* 16, 3548–3552. <https://doi.org/10.1002/cmdc.202100483>.
- Martina, M.G., Sannio, F., Crespan, E., Pavone, M., Simoncini, A., Barbieri, F., Perini, C., Pesce, E., Maga, G., Pedemonte, N., Docquier, J.D., Radi, M., 2022. Towards innovative antibacterial correctors for cystic fibrosis targeting the lung microbiome with a multifunctional effect. *ChemMedChem* 17, e202200277. <https://doi.org/10.1002/cmdc.202200277>.
- McPhail, J.A., Burke, J.E., 2023. Molecular mechanisms of PI4K regulation and their involvement in viral replication. *Traffic* 24, 131–145. <https://doi.org/10.1111/tra.12841>.
- Mathe, G., Cagno, V., 2021. Clinical severe acute respiratory syndrome coronavirus 2 isolation and antiviral testing. *Antivir. Chem. Chemother.* 29, 20402066211061063. <https://doi.org/10.1177/20402066211061063>.
- Mejdrová, I., Chalupská, D., Kögler, M., Šála, M., Pláčková, P., Baumlová, A., Hřebabecý, H., Procházková, E., Dejmeck, M., Strunin, D., Weber, J., Lee, G., Birkus, G., Mertlíková-Kaiserová, H., Boura, E., Nencka, R., 2015. Highly selective phosphatidylinositol 4-kinase IIIβ inhibitors and structural insight into their mode of action. *J. Med. Chem.* 58, 3767–3793. <https://doi.org/10.1021/acs.jmedchem.5b00499>.
- Mejdrová, I., Chalupská, D., Pláčková, P., Müller, C., Šála, M., Klíma, M., Baumlová, A., Hřebabecý, H., Procházková, E., Dejmeck, M., Strunin, D., Weber, J., Lee, G., Matoušová, M., Mertlíková-Kaiserová, H., Ziebuhr, J., Birkus, G., Boura, E., Nencka, R., 2017. Rational design of novel highly potent and selective phosphatidylinositol 4-kinase IIIβ (PI4KB) inhibitors as broad-spectrum antiviral agents and tools for chemical biology. *J. Med. Chem.* 60, 100–118. <https://doi.org/10.1021/acs.jmedchem.6b01465>.
- Meliá, C.E., van der Schaar, H.M., Lyoo, H., Limpens, R., Feng, Q., Wahedi, M., Overheul, G.J., van Rij, R.P., Snijder, E.J., Koster, A.J., Barcena, M., van Kuppeveld, F.J.M., 2017. Escaping host factor PI4KB inhibition: enterovirus genomic RNA replication in the absence of replication organelles. *Cell Rep.* 21, 587–599. <https://doi.org/10.1016/j.celrep.2017.09.068>.
- Nainwal, N., 2022. Treatment of respiratory viral infections through inhalation therapeutics: challenges and opportunities. *Pulm. Pharmacol. Ther.* 77, 102170. <https://doi.org/10.1016/j.pupt.2022.102170>.
- Ooi, M.H., et al., 2010. Clinical features, diagnosis, and management of enterovirus 71. *Lancet Neurol* 9 (11), 1097–1105.
- Poelaert, K.C.K., Van Kleef, R.G.D.M., Liu, M., Van Vliet, A., Lyoo, H., Gerber, L.-S., Narimatsu, Y., Büll, C., Clausen, H., De Vries, E., Westerink, R.H.S., Van Kuppeveld, F.J.M., 2023. Enterovirus D-68 infection of primary rat cortical neurons: entry, replication, and functional consequences. *mBio* 14, e00245. <https://doi.org/10.1128/mbio.00245-23>, 23.
- Routlin, P.S., Murer, L.P., Greber, U.F., 2018. A single point mutation in the rhinovirus 2B protein reduces the requirement for phosphatidylinositol 4-kinase class III beta in viral replication. *J. Virol.* 92. <https://doi.org/10.1128/JVI.01462-18>.
- Spickler, C., Lippens, J., Laberge, M.K., Desmeules, S., Bellavance, E., Garneau, M., Guo, T., Hucke, O., Leyssen, P., Neyts, J., Vaillancourt, F.H., Decor, A., O'Meara, J., Franti, M., Gauthier, A., 2013. Phosphatidylinositol 4-kinase III beta is essential for replication of human rhinovirus and its inhibition causes a lethal phenotype in vivo. *Antimicrob. Agents Chemother.* 57, 3358–3368. <https://doi.org/10.1128/AAC.00303-13>.
- Syage, A., Pachow, C., Cheng, Y., Mangale, V., Green, K.N., Lane, T.E., 2023. Microglia influence immune responses and restrict neurologic disease in response to central nervous system infection by a neurotropic murine coronavirus. *Front. Cell. Neurosci.* 17, 1291255. <https://doi.org/10.3389/fncel.2023.1291255>.
- Tassini, S., Sun, L., Lanko, K., Crespan, E., Langron, E., Falchi, F., Kissova, M., Armijos-Rivera, J.I., Delang, L., Mirabelli, C., Neyts, J., Pieroni, M., Cavalli, A., Costantino, G., Maga, G., Vergani, P., Leyssen, P., Radi, M., 2017. Discovery of multitarget agents active as broad-spectrum antivirals and correctors of cystic fibrosis transmembrane conductance regulator for associated pulmonary diseases. *J. Med. Chem.* 60, 1400–1416. <https://doi.org/10.1021/acs.jmedchem.6b01521>.
- Tassini, S., Langron, E., Delang, L., Mirabelli, C., Lanko, K., Crespan, E., Kissova, M., Tagliavini, G., Fontò, G., Bertoni, S., Palese, S., Giorgio, C., Ravanetti, F., Ragionieri, L., Zamperini, C., Mancini, A., Dreassi, E., Maga, G., Vergani, P., Neyts, J., Radi, M., 2019. Multitarget CFTR modulators endowed with multiple beneficial side effects for cystic fibrosis patients: toward a simplified therapeutic approach. *J. Med. Chem.* 62, 10833–10847. <https://doi.org/10.1021/acs.jmedchem.9b01416>.

- Van Der Schaar, H.M., Leyssen, P., Thibaut, H.J., De Palma, A., Van Der Linden, L., Lanke, K.H.W., Lacroix, C., Verbeken, E., Conrath, K., MacLeod, A.M., Mitchell, D.R., Palmer, N.J., Van De Poël, H., Andrews, M., Neyts, J., Van Kuppeveld, F.J.M., 2013. A novel, broad-spectrum inhibitor of enterovirus replication that targets host cell factor phosphatidylinositol 4-kinase III $\beta$ . *Antimicrob. Agents Chemother.* 57, 4971–4981. <https://doi.org/10.1128/AAC.01175-13>.
- Wu, G.-H., Lee, K.-M., Kao, C.-Y., Shih, S.-R., 2023. The internal ribosome entry site determines the neurotropic potential of enterovirus A71. *Microb. Infect.* 25, 105107. <https://doi.org/10.1016/j.micinf.2023.105107>.
- Yang, N., Ma, P., Lang, J., Zhang, Y., Deng, J., Ju, X., Zhang, G., Jiang, C., 2012. Phosphatidylinositol 4-kinase III $\beta$  is required for severe acute respiratory syndrome coronavirus spike-mediated cell entry. *J. Biol. Chem.* 287, 8457–8467. <https://doi.org/10.1074/jbc.M111.312561>.